PREDICTION OF THE ORBITAL EVOLUTION FOR LEO GEODETIC SATELLITES

A. Bezděk

Astronomical Institute, Academy of Sciences of the Czech Republic, Ondřejov, Czech Republic – bezdek@asu.cas.cz

KEY WORDS: Atmosphere, Geodesy, Space, Modelling, Prediction, Simulation, Satellite, Theory

ABSTRACT:

The orbital changes of a LEO (low Earth orbit) satellite are – apart from the gravitational field forces – mainly influenced by atmospheric drag, which causes the satellite to lose energy and to descend. To model accurately the atmospheric drag is a quite complex task. We will discuss the uncertainty in predicting the orbital evolution of a LEO satellite for longer periods of time, using the semianalytical theory of LEO satellite motion. Examples of applying this procedure to current geodetic satellites will be given.

1. INTRODUCTION

The motivation for this paper originated in the collaboration of the author with space geodesists who needed a prediction of future passes of Grace satellites through orbital resonances. This is important, because degradation was observed in the gravity solution accuracy when the Grace satellites passed through the 61:4 resonance in September 2004 (Wagner et al., 2005). Estimating the orbital evolution of LEO satellites (in *low Earth orbits*, i.e. with heights under ca 2000 km) is specific, because in modelling atmospheric drag there are important sources of uncertainties that cannot be left aside, when doing a long-term prediction. Generally, we would like to show what the most important error sources in modelling atmospheric drag are, and, more specifically, we will present the results of the above-mentioned future prediction problem using a semianalytical theory of motion for LEO satellites.

1.1 Theories of motion for LEO satellites

To characterize the semianalytical method used to calculate the long-term prediction, it is useful to schematically group theories of motion for LEO satellites into (Hoots and France, 1987):

(i) *Analytical* – Historically, when the first artificial satellites appeared in the late 1950's, the methodology used in celestial mechanics was applied to describe their motion. While the analytical methods were rather successful when dealing with forces of gravitational origin, an adequate analytical description of the atmospheric drag proved to be extremely difficult (Brouwer, 1963; King-Hele, 1964, 1992). In the analytical approach, the forces acting on LEO satellites were divided according to the *theory of perturbations*. The dominant force in the vicinity of the Earth is that induced by the geopotential monopole. The other forces are small compared to this major acceleration, so the Kepler ellipse of LEO satellites changes slowly in time under the influence of perturbations. Among these, we find gravitational perturbations induced by higher geopotential terms, action of Sun and Moon, tides, etc. In the analytical way, one can approximately model the nongravitational perturbations as well, for satellites under ca 400 km the dominant force being the atmospheric drag. In order to be able to solve the equations of motion analytically, one is forced to do many approximations. On the other hand, from the computational point of view, having an analytical solution at hand, we can jump from the initial conditions to the new state vector at any time in a single leap, which makes the computation extremely fast.

(ii) *Numerical* – In this case, no approximations to the formulation of physical forces are necessary, but the orbital evolution is time-consuming and computationally intensive. The accuracy of the resulting orbit depends on that of the physical models used in the calculation.

(iii) *Semianalytical* – In this case, the perturbation accelerations are usually averaged over one revolution, which results in much more speedy orbital evolution calculations than the numerical ones. Approximations are necessary, but less stringent than for analytical theories. Typical applications for semianalytical theories: long-term evolution, lifetime estimates.

1.2 Nongravitational forces

To get some idea about the nongravitational forces at LEO heights and their magnitudes, we will look at Fig. 1. In the figure, there are two revolutions of the Castor satellite (1975-039B) between 270 km at perigee and 1170 km at apogee (the bottom panel). At the centre of mass of the satellite, a microaccelerometer was placed, which measured the nongravitational forces that acted on the satellite as it passed along its orbit. Near the perigee, under ca 400 km, by far the largest acceleration is caused by the atmospheric drag (see the top panel). The passes through the perigee take place at midnight local time (the middle panel). As the upper atmosphere absorbs the solar UV radiation, its density increases during daytime by a factor of 2–4, the relative peakedness of atmospheric drag is even more pronounced. The second largest acceleration in Fig. 1 is the direct solar radiation pressure. The inclination of the Castor's orbital plane being 30°, the satellite enters the shadow of the Earth during each revolution. At time 1900 s, it is clearly distinguishable that the satellite enters the shadow, the direct solar radiation pressure steeply disappears. The satellite is sunlit again at 3600 s, but there the drag is 20 times greater than the radiation pressure. Accelerations induced by radiation pressures may significantly perturb the orbit, provided the satellites have very large surface and low mass, e.g. balloon-like satellite Explorer 9. This is not the case of geodetic satellites, which are usually designed to minimize the effects of nongravitational forces. This dominance of atmospheric drag below 400 km over other nongravitational forces is generally valid for any LEO satellite down to 100–150 km, the lower edge of the thermosphere, where nearly all the satellites fall out of orbit and burn up.

2. ATMOSPHERIC DRAG

2.1 Effects on LEO satellites

We begin this section on the most important perturbing force at LEO heights by showing its practical manifestations, which are common to all LEO satellites. In Fig. 2 and 3 it is clear that under the influence of atmospheric drag the satellite slowly spirals down

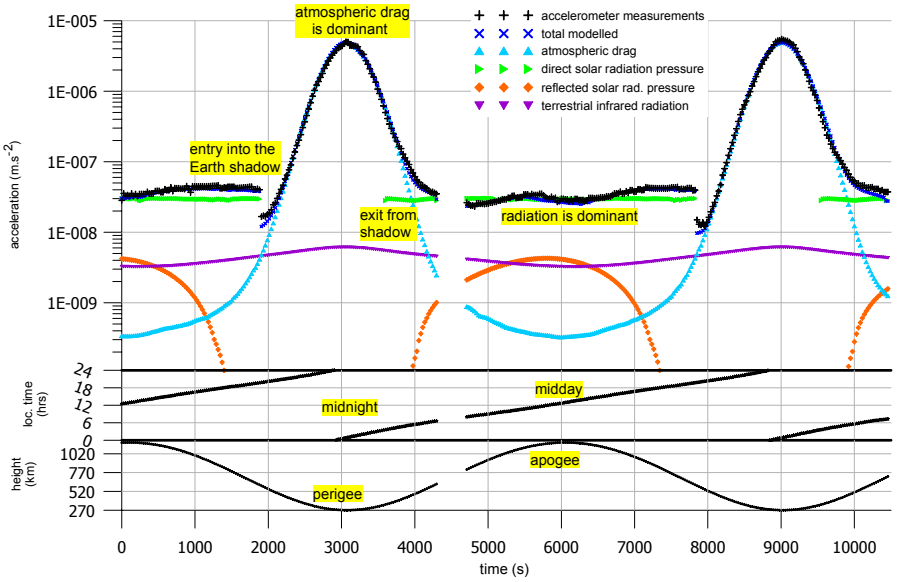

Figure 1. Microaccelerometer measurements of nongravitational accelerations during two orbits of satellite Castor on 18 June 1976. (Lack of data between 4300–4700 s is probably due to telemetry communication.)

towards the denser layers of the atmosphere. In the figures, it is obvious that the apogee height reduces more quickly than that at perigee. Due to exponential decrease in the air density and higher speed at perigee, the satellite is dragged mainly around the perigee, thus losing the velocity and energy for the next journey to the apogee. In this way we may understand that atmospheric drag secularly diminishes both semimajor axis a and eccentricity e, the heights at perigee h_p and apogee h_a being in a first approximation given by $h_p = a(1-e)$, $h_a = a(1+e)$.

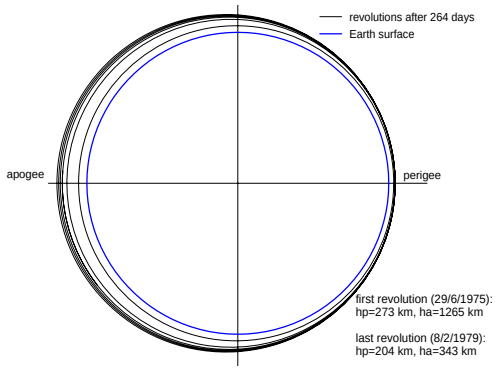

Figure 2. Decrease in height of the Castor satellite during its lifetime due to atmospheric drag.

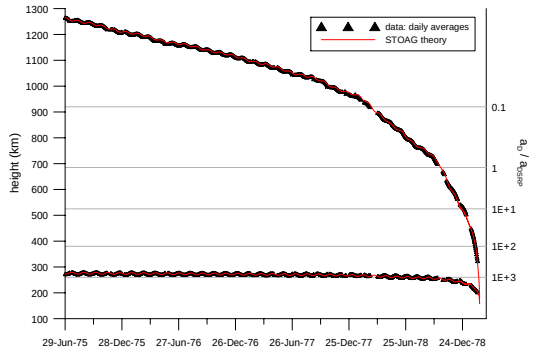

Figure 3. Height at perigee and apogee of satellite Castor.

2.2 Uncertainties in the atmospheric drag

Atmospheric drag is a vector directed opposite to velocity **v** of the satellite with respect to the atmosphere at rest, of the magnitude

$$a_D = \frac{1}{2} C_D \frac{S}{m} \rho v^2 , \qquad (1)$$

where C_D is the drag coefficient, (S/m) is the area-to-mass ratio of the satellite and ρ the thermospheric density. To make an overview of the sources of uncertainties in calculating the drag, using small increments of quantities in Eq. (1) we will obtain for relative uncertainties

$$\frac{\Delta a_D}{a_D} = \frac{\Delta C_D}{C_D} + \frac{\Delta (S/m)}{(S/m)} + \frac{\Delta \rho}{\rho} + 2\frac{\Delta v}{v} . \qquad (2)$$

In our present discussion we will leave aside the uncertainties in the area-to-mass ratio and velocity, and describe in more detail those in the drag coefficients and atmospheric density, which represent the specific problems connected with LEO satellites calculations.

2.3 Drag coefficient

The drag coefficient C_D in Eq. (1) comprises the physics of the interaction between the atmospheric constituents at a given height and the material from which a surface element of the satellite is made. Over the years since the beginning of the space age, many theoretical models of this interaction, together with assumptions about the underlying physical processes, were put forward, being more or less based on the laboratory measurements. However, it is now generally recognized that realistic in-orbit conditions cannot be obtained in the laboratory (Moe and Moe, 2005), and we are thus left with some $\pm 5\,\%$ uncertainty in C_D (King-Hele, 1992). As an illustration, in Fig. 4 two different models of C_D for spherical satellites are shown, together with the traditional estimate $C_D = 2.2$ computed by Cook (1965).

Taking into consideration the uncertainty in C_D and the fact that satellite surfaces are usually covered with different materials, each having different C_D, in practice one usually fits the ballistic coefficient,

$$B \equiv C_D \frac{S}{m} , \qquad (3)$$

to the real data. It is clear that such a fitted parameter encompasses the uncertainties and mismodelling errors of the other terms on the right-hand side of Eq. (2).

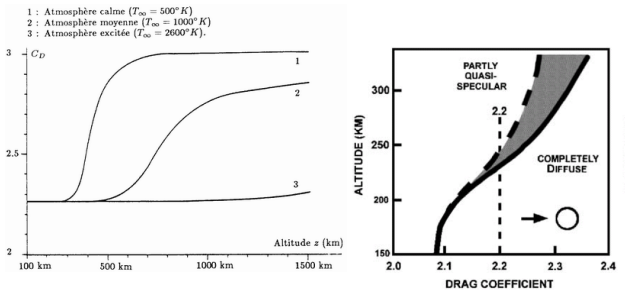

Figure 4. Examples of different theoretical drag coefficients for spherical satellites (on the left a graph taken from Zarrouati, 1987, on the right from Moe and Moe, 2005).

3. ATMOSPHERIC DENSITY

This section will be devoted to the neutral atmospheric density, a subject of intensive research (Proelss, 2004).

3.1 Thermosphere

As a sort of reminder, in Fig. 5 we can see the vertical profile of atmospheric temperature, whose steep growth above 100 km and very high temperatures gave the name to the region, where space flights take place, to the "thermosphere". Relevant to our present discussion is the appreciable variation in the thermospheric temperature in the course of the solar activity cycle. The same phenomenon of very marked changes in the thermospheric density may be seen in Fig. 6. As is clearly visible in the figures, such changes due to the level of solar activity and to local time do not exist near the Earth's surface, and they were absolute surprise at the beginning of the space age (King-Hele, 1992). The cause thereof is the absorption of solar UV radiation, which is the main energy source for the upper atmosphere and brings about its high temperatures. Even the day-night cycle causes the thermospheric density to vary with a factor of tens of percent (Fig. 6).

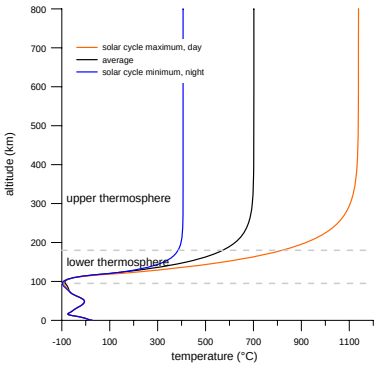

Figure 5. Temperature altitude profile in the atmosphere.

3.2 Cycle of solar activity

The most problematic part of LEO orbital predictions is the cycle of solar activity (CSA). In Fig. 7 we see the variations in solar radio flux at 10.7 cm that is used as a proxy for solar UV. While the total radiation energy over all wavelengths coming from the Sun to the Earth is virtually constant, 1.37 kW/m^2, variations being less than 0.3 % (Proelss, 2004), the solar UV radiation changes

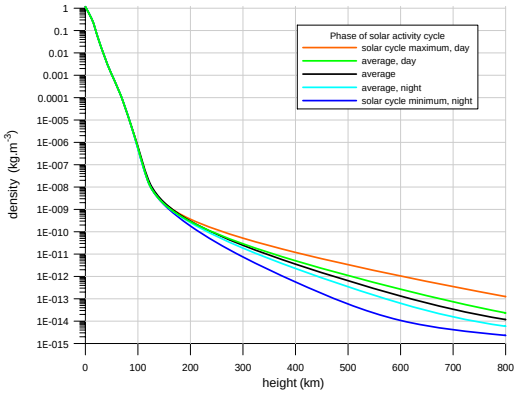

Figure 6. Variations in the atmospheric density within 0–800 km.

rather markedly following the 11-year CSA, which is well-known from the study of sunspots since the 19th century. Problems arise, when we want to predict the CSA, because, so far, solar physicists are unable to theoretically predict the exact date of beginning of the next cycle, nor its exact daily progress. For example, the length of the cycles in Fig. 7 varies between 10.0–11.4 years and their shape is different from one cycle to another, so any numerical method to model them encounters difficulties. Another problem is the variability of indices that are used to parameterize the CSA (Fig. 8). The exact date of the CSA minimum and maximum varies according to the index used, thus creating another type of uncertainty.

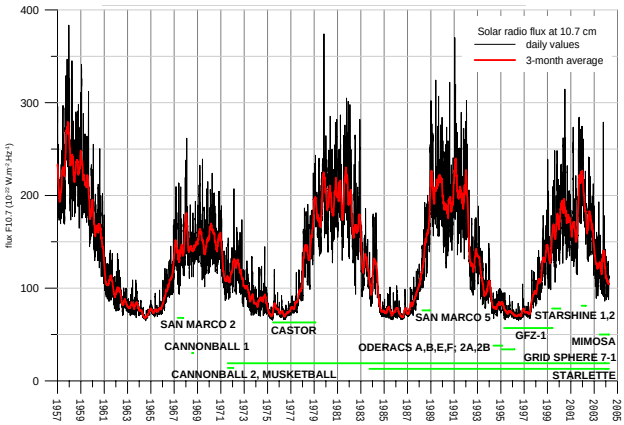

Figure 7. Solar radio flux at 10.7 cm wavelength measured on the ground. Satellites used for testing the STOAG theory.

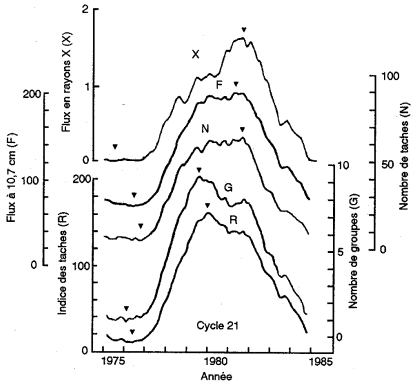

Figure 8. Dates of maxima and minima of one 11-year solar activity cycle using different indices: X-rays, 10.7 cm, sunspot numbers (Lantos, 1997).

3.3 Geomagnetic storms

Apart from the solar UV flux variations, other source of distinct "peaks" in the thermospheric density is connected with the irregular variations of the terrestrial magnetic field, namely with the geomagnetic storms (see Fig. 9). The geomagnetic storms are induced by energetic particles from solar wind that enter the geomagnetic field with high speeds and dissipate their extra kinetic energy to heat. This creates higher atmospheric densities, hence, a higher drag on satellites. Similarly to the solar UV radiation, on a longer-term basis the arrival dates of these energetic particles are irregular and cannot be predicted.

During geomagnetic storms the energetic particles perturb the terrestrial ionosphere as well, in this way creating *ranging errors in the GPS positioning*. Storms frequently cause rapid fluctuations of the amplitude and phase of the GPS signals (scintillations), which may prevent a position-fixing altogether (Proelss, 2004, p. 445).

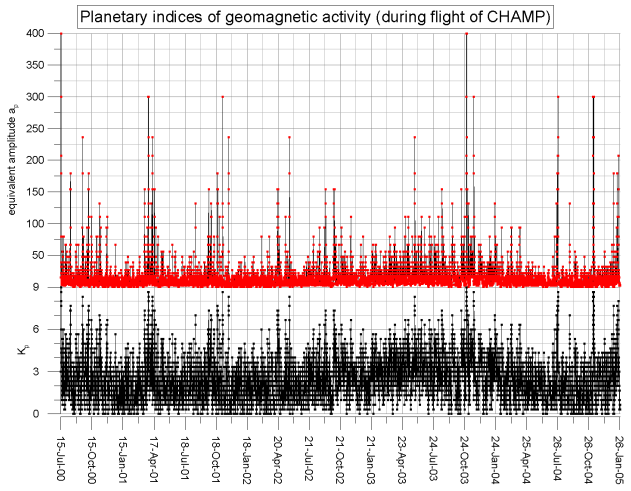

Figure 9. Planetary indices of geomagnetic activity (during flight of CHAMP satellite). Minor geomagnetic storm is defined, when 29<ap<50, major for 50≤ap<100, severe for ap≥100.

3.4 Models of the thermospheric density

Similarly to the theories of motion, models of the thermospheric neutral density may be grouped according to their physical content and computational demands. In orbital dynamics, the semiempirical models (e.g. Jacchia, MSIS or DTM model series, for references see Bezděk and Vokrouhlický, 2004) are used for the most detailed description of the neutral thermosphere, and oversimplified analytical models for quick analytical computations. The semiempirical models are based on the physical assumptions, some of which are rather simplified (e.g. the diffusive equilibrium of atmospheric components above 100 km), and take into account the dynamic variation of the thermosphere due to solar and geomagnetic activity. The numerical quadrature of the diffusion equations can be very CPU demanding, so several mathematically efficient approximations to the semiempirical models have been proposed (e.g. de Lafontaine and Hughes, 1983; Gill, 1996). The analytical models of the thermosphere are usually based on exponential or power function representation of the total density, sometimes with a refinement e.g. for the Earth oblateness or the altitude dependent scale height (ECSS, 2000; Hoots and France, 1987; King-Hele, 1964). Let us remark that there are also fully physical models of the upper atmosphere (based on the transport equations), but they are too complicated for use in orbital dynamics and show no quantitative advantage over semiempirical models (Marcos, 2002).

Considering the accuracy of the neutral atmospheric density models, $\Delta\rho/\rho$ in Eq. (2), the answer is rather disappointing. Since the late 1970's up to now, the standard deviation of all the models remains around the 15 % level, on condition that we use the measured data of solar and geomagnetic activity (Owens et al., 2000). This uncertainty is, apart from that connected with C_D, another reason for the ballistic coefficient (3) to be fitted to the orbital data, as was noted in Sec. 2.3.

4. THE STOAG THEORY

The STOAG (Semianalytic Theory of mOtion under Air drag and Gravity) theory of motion for LEO satellites may be divided into two parts: the perturbations due to drag are treated semianalytically, those due to the geopotential analytically. The theory originated from the semianalytical theory of motion of an artificial satellite in the Earth atmosphere (Sehnal and Pospíšilová, 1991), which was based on the specific formula of the thermospheric total density model TD88 (Sehnal and Pospíšilová, 1988). In principle, the model TD88 is analytic (a sum of exponential functions), but by means of an appropriate weighting of the base exponentials it takes into account the physical parameters having influence on the thermospheric density (solar flux, geomagnetic activity, diurnal and seasonal variations, geographic latitude). The TD88's free parameters are adjustable to fit the model or real density data, so TD88 may be viewed as a mathematical approximation to virtually any semiempirical model. On the other hand, the structure of TD88 is devised in such a way that it allows the osculating equations of motion to be analytically integrated over one revolution of the satellite, which permits one to use the averaged equations of motion.

The original version of the theory has been substantially extended. In the present version, the theory comprises the long-period and secular gravitational perturbations due to the zonal harmonics J_2–J_9 of the geopotential as well as the long-period lunisolar perturbations. In order to test the theory predictions against passive spherical satellites, which often have near-circular orbits, the theory uses the eccentricity nonsingular elements. For mathematical definition and implementation comments regarding the STOAG theory, please refer to the more extensive paper (Bezděk and Vokrouhlický, 2004).

The STOAG theory may be applied in situations, where one needs a quick orbital propagator for LEO objects, which are significantly influenced by air drag, but undergo the long-term gravitational variations as well (e.g. mission planning, lifetime prediction, space debris dynamics). Compared to the analytical theories including air drag (e.g. Brouwer and Hori, 1961; King-Hele, 1964), the STOAG theory embraces the dynamics of the thermosphere via the measured (or predicted) solar activity indices.

To validate the STOAG theory we compared its predictions with passive (quasi)spherical satellites flown in the past (Fig. 7), when solar and geomagnetic activity is known and the deviations of the "predicted" and measured orbital elements come from the theory itself. Each time we started with only one initial set of orbital elements, which was then propagated further on. The unavoidable uncertainties in the initial orbital elements and in the physical characteristics of a satellite were relegated to the "C_D-induced" confidence interval, which we defined to quantify the uncertainty in our prediction of the orbital elements evolution. An example of a geodetic satellite used to validate the STOAG theory is in Fig. 10.

For a detailed discussion, other test satellites and application examples, refer to Bezděk (2004); Bezděk and Vokrouhlický (2004).

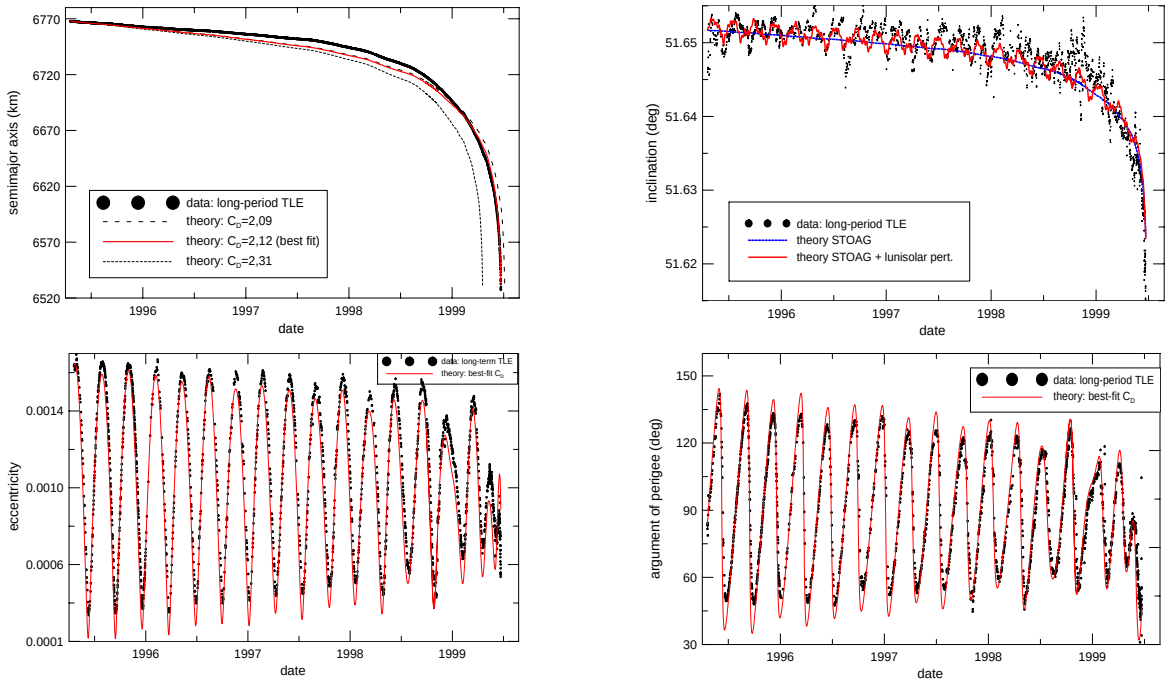

Figure 10. Long-term evolution of the orbital elements of geodetic satellite GFZ-1 (1995-020A). The steady decrease in the semimajor axis is caused by the action of air drag, leading finally to the decay of the satellite out of its orbit. The inclination displays the overall decrease caused by air drag, the long-period oscillations are predominantly induced by the lunisolar perturbations. Due to the low eccentricity, the nonsingular elements were used throughout the whole lifetime, which couple the gravitational and drag perturbations in the eccentricity and argument of perigee. The theory shows quite well the variations caused by the odd zonal harmonics of the geopotential, leading to the libration of the argument of perigee around 90°, combined with the action of the drag that modifies the amplitude of the variations.

The online calculation, Fortran code as well as these references are available on the website: http://www.asu.cas.cz/˜bezdek/density_therm/pohtd/.

5. PREDICTION OF PASSES THROUGH RESONANCES FOR THE GRACE SATELLITES

Now we want to make a prediction of future orbital evolution of Grace satellites in order to assess the dates of their passing through important orbital resonances. For this purpose, we chose the Grace A satellite. To model its motion using the STOAG theory, we made several approximations. We take the satellite to be a passively flying body with a constant ballistic coefficient. This is, of course, a rather simplistic view, as the orientation of the satellite is corrected continuously by the action of magnetic torque rods and from time to time by thrusters (Herman et al., 2004), but we will suppose that its surface-to-mass ratio with respect to the direction of motion remains constant on average. As the orbital data we used the two-line elements computed by GFZ Potsdam.

5.1 Test of the method for 2005

To have an idea of how good our prediction of the semimajor axis evolution is, we made several tests, when we predicted the orbital evolution of semimajor axis and compared the results with the actual data. Here, we will show the prediction made in Feb. 2005 for the rest of the year, together with the actual orbital data.

In accordance with the discussion in Sec. 2.3, first we fitted the ballistic coefficient B of the Grace satellite to the actual semimajor axis a data in 2004 (Fig. 11), and then we used it for estimating the semimajor axis evolution in 2005. Each day, we adjusted B, so that the change in a computed by the STOAG theory matches the actual change taken from the two-line elements. We made no optimization in the two-line elements, just linear interpolation between the neighbouring element sets. In Fig. 11, sometimes the daily values of the fitted B change wildly, as B fitted in this way comprises all the uncertainties not only of the STOAG theory, but of the measured data too. This interpretation is supported by low value of the relative standard deviation of the average, 1.8 %, and is in accordance with the above stated assumption about the relatively constant ballistic coefficient of the satellite.

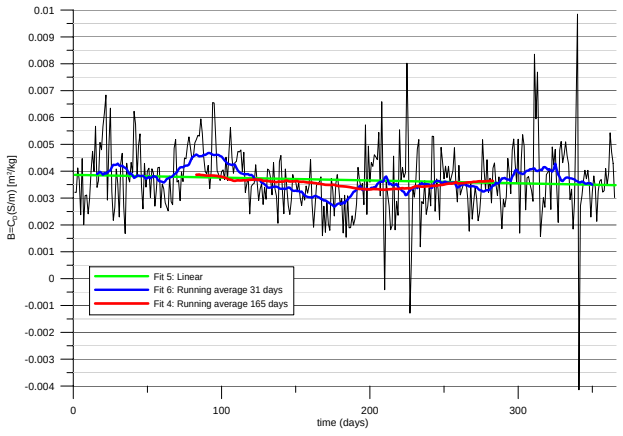

Figure 11. Fitting the ballistic coefficient of the Grace A satellite in 2004. The average value of B is 0.0037, relative std. deviation 34 %, relative std. deviation of the average 1.8 %.

To represent the future evolution of solar activity we used a model with three levels of averaged flux $F10.7$ at 10.7 cm (Fig. 12). The maximum and minimum curves were defined to be the upper and lower limits of 3-month average flux values from the preceding cycles (Fig. 7). In Fig. 12 it is evident that the new cycle will start

somewhere around 2007–2009.

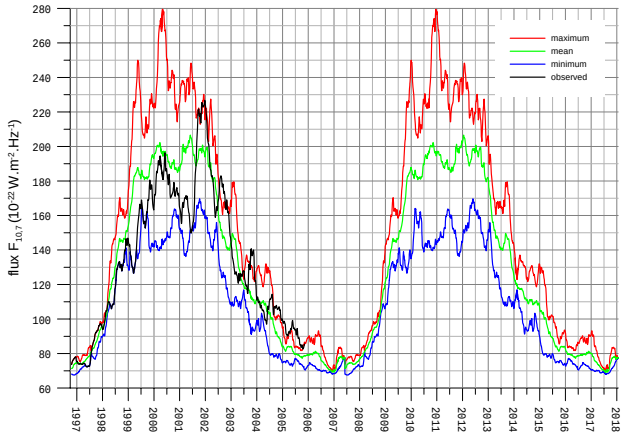

Figure 12. Model of averaged $F10.7$ flux for period 1996–2018.

The resulting curves for the semimajor axis evolution estimate for 2005 are in Fig. 13. With the mean level of modelled solar activity (SA) we used the mean fitted ballistic coefficient B (Fig. 11). To have a reasonable uncertainty band, with the minimum SA level we took B reduced by 2 %, which corresponds to the standard deviation of B, with the maximum SA level we augmented B by 2 %. The limiting curves in Fig. 13 are in fact the main result of any orbital evolution prediction. In this case, the observed semimajor axis data fits rather well into the theoretical uncertainty band, but one must not forget that we are always dependent on the vagaries of the Sun in its UV activity.

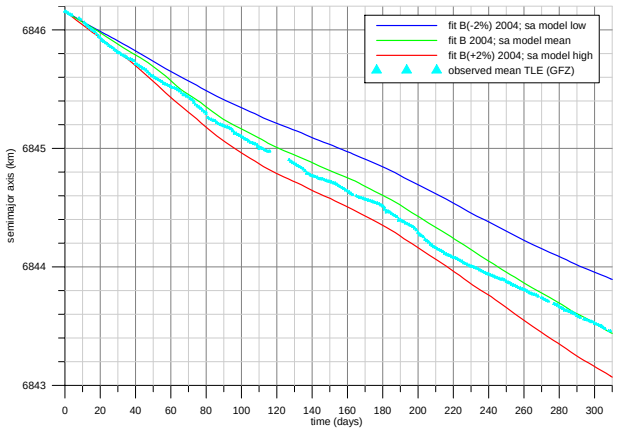

Figure 13. Testing the prediction of the orbital elements evolution for Grace A (24 Feb–31 Dec 2005).

5.2 Passes of Grace A through resonances in the near future

In a way analogous to the 2005 test, we fitted the ballistic coefficient to the 2005 orbital data, and made the subsequent calculations. In Fig. 14 we see the prediction for the semimajor axis for period 2006–2009, together with approximate dates of passes through resonances computed by the STOAG theory. Namely, the first pass through an important resonance 107:7 falls to the period 08/2007–03/2008 and 46:3 to 08/2009–03/2010. Not shown in figures are the following resonances, 77:5 in 04/2010–08/2011 and 31:2 in 12/2010–02/2013, but at this time the Grace mission will probably be no more in the active phase.

5.3 Uncertainty in lifetime predictions

In Fig. 15 we see the STOAG lifetime prediction. The wide range in the lifetime prediction results primarily from our inability to

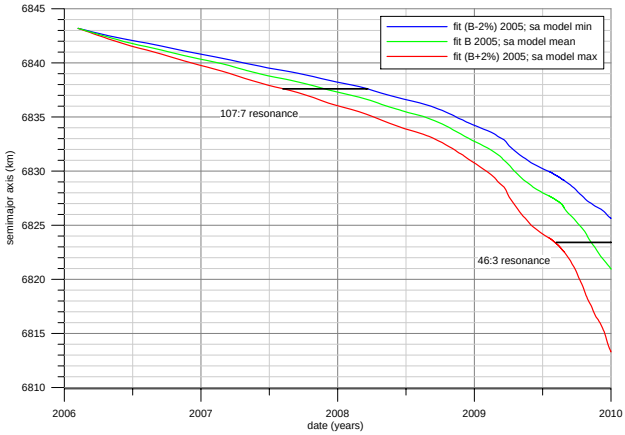

Figure 14. Prediction of the orbital elements evolution by STOAG theory for Grace A (Feb 2006–Dec 2009).

predict the date, when the new solar activity cycle begins. This very large uncertainty will reduce considerably, when we know the actual starting date of the new cycle. This statement is supported by numerical simulations of orbital lifetime predictions made by Owens et al. (2000), where the authors conclude that "the uncertainties associated with our current talent for estimating future solar activity significantly outweighs the sensitivity due to even large errors in drag coefficient estimation".

As another illustration of the uncertainty in the lifetime estimates, we may take the Castor satellite (Fig. 3). Satellite Castor flew in 1975–1979, and as may be seen in Fig. 7, similarly to Grace, the next cycle of solar activity began near the end of its flight. We may repeat the "lifetime prediction" for Castor, as if we had no knowledge about the actually observed $F10.7$ solar flux. For this case of unknown both C_D and $F10.7$ we get ± 27 % uncertainty in the theoretical lifetime prediction. When we use the actually measured $F10.7$, the uncertainty persisting only in C_D (in this case we took ± 5 %), the theory gives the length of lifetime with ± 2.2 %.

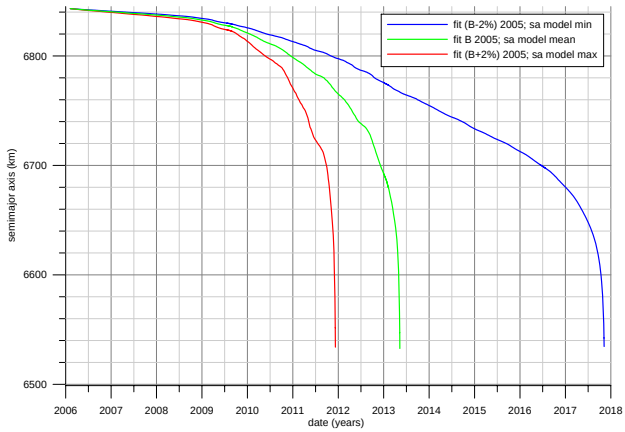

Figure 15. Prediction of orbital elements evolution by STOAG theory for Grace A (Feb 2006 till the end of orbital lifetime).

6. CONCLUSIONS

The aim of this paper was to give the reader some insight into the problem of predicting the orbital evolution for LEO satellites over longer periods of time. At LEO heights, the main limiting factor in the accuracy of such a prediction is the atmospheric

drag. The uncertainties caused by drag lie on the one hand in the not yet well modelled interaction between the satellite surface and thermospheric particles, thus reducing the precision of orbital estimates to the several percent order. But the largest unknown is the future behaviour of solar activity, where so far we are not able to predict the beginning nor the shape and duration of the next cycle of solar activity with a necessary level of precision. The resulting uncertainties may climb to tens of percent or more in the estimated lifetimes. The concrete motivation of the paper was the estimation of future passes of Grace satellites through orbital resonances. This problem was solved with the attainable accuracy using the semianalytical theory of motion for LEO satellites.

ACKNOWLEDGEMENTS

The author wishes to express his gratitude to the organizers of the symposium for financial support.

References

Bezděk, A., 2004. Semianalytic theory of motion for LEO satellites under air drag. 18th International Symposium on Space Flight Dynamics, *ESA SP-548*, 615–620 (http://www.asu.cas.cz/˜bezdek/density_therm/pohtd/).

Bezděk, A., Vokrouhlický, D., 2004. Semianalytic theory of motion for close-Earth spherical satellites including drag and gravitational perturbations. *Planet. Sp. Sci.* 52(14), 1233–1249.

Brouwer, D., 1963. Review of celestial mechanics. *Annual Rev. of Astron. and Astroph.* 1, 219–234.

Brouwer, D., Hori, G., 1961. Theoretical evaluation of atmospheric drag effects in the motion of an artificial satellite. *Astron. J.* 66, 193–225.

Cook, G. E., 1965. Satellite Drag Coefficients. *Planet. Space Sci.* 13, 929–945.

de Lafontaine, J., Hughes, P., 1983. An Analytic Version of Jacchia's 1977 Model Atmosphere. *Celes. Mech.* 29, 3–26.

ECSS, 2000. *Space engineering. Space environment*. European Cooperation for Space Standardization, ESA-ESTEC Publications Division, ECSS-E-10-04A.

Gill, E., 1996. Smooth Bi-Polynomial Interpolation of Jacchia 1971 Atmospheric Densities For Efficient Satellite Drag Computation. DLR-GSOC IB 96-1.

Herman, J., Presti, D., Codazzi, A., Belle, C., 2004. Attitude Control for GRACE. 18th International Symposium on Space Flight Dynamics, *ESA SP-548*, 27–32.

Hoots, F. R., France, R. G., 1987. An analytic satellite theory using gravity and a dynamic atmosphere. *Celest. Mech.* 40, 1–18.

King-Hele, D. G., 1964. *Theory of satellite orbits in an atmosphere*. Butterworth, London.

King-Hele, D. G., 1992. *A Tapestry of Orbits*. Cambridge University Press, Cambridge.

Lantos, P., 1997. *Le Soleil en face*. Masson, Paris.

Marcos, F. A., 2002. AFRL Satellite Drag Research. The 2002 Core Technologies for Space Systems Conference, Colorado Springs, Colorado, November 19–21.

Mazanek, D., 2000. GRACE Mission Design: Impact of Uncertainties in Disturbance Environment and Satellite Force Models. AAS/AIAA Space Flight Mechanics Meeting, Clearwater, Florida, 23–26 Jan, AAS 00-163.

Moe, K., Moe, M. M., 2005. Gas-surface interactions and satellite drag coefficients. *Planet. Sp. Sci.* 53, 793–801.

Owens, J. K., Vaughan, W. W., Niehuss, K. O., Minow, J., 2000. Space Weather, Earth's Neutral Upper Atmosphere (Thermosphere), and Spacecraft Orbital Lifetime/Dynamics. *IEEE Transactions on plasma science* 28 (6), 1920–1930.

Proelss, G. W., 2004. *Physics of the Earth's Space Environment: An Introduction*. Springer-Verlag, Berlin, Heidelberg.

Sehnal, L., Pospíšilová, L., 1988. Thermospheric model TD88. Preprint No. 67 of the Astron. Inst. Czechosl. Acad. Sci.

Sehnal, L., Pospíšilová, L., 1991. Lifetime of the ROHINI A satellite. *Bull. Astron. Inst. Czechosl.* 42, 295–297.

Wagner, C. A., McAdoo, D. C., Klokočník, J., Kostelecký, J., 2005. Degradation of Grace Monthly Geopotentials in 2004 Explained. AGU Spring Meeting Abstracts, 4.

Zarrouati, O., 1987. *Trajectoires Spatiales*. Cepaudes-Editions, Toulouse.